Entropically-Driven Formation of Smectic A1, A2, and A3 phases in Binary Mixtures of Rigid-Rod Helical Polysilanes with Different Molecular Weights

Kento Okoshi,*,† Akiko Suzuki,† Masatoshi Tokita,† Michiya Fujiki,‡ and Junji Watanabe*,†

Department of Polymer Chemistry, Tokyo Institute of Technology, Ookayama, Meguro-ku, Tokyo 152-8552, Japan, and Graduate School of Materials Science, Nara Institute of Science and Technology, 8916-5 Takayama, Ikoma, Nara 630-0101, Japan

Received January 9, 2009; Revised Manuscript Received March 25, 2009

ABSTRACT: The smectic liquid crystal arrangements of binary mixtures of rod-like polymers, i.e., poly[*n*-decyl-(*S*)-2-methylbutylsilane]s, with narrow molecular weight distributions, were investigated by synchrotron radiation small-angle X-ray scattering (SR-SAXS) and atomic force microscopy (AFM) analyses. Depending on the molecular weight ratio, *r* (higher molecular weight/lower molecular weight), and the mixing ratio, three types of smectic phases are formed with different accommodations by two polymers. In the binary mixture of the shorter and longer polymers with the lower *r* values of 1.0−1.7, the two polymers are randomly mixed within a layer, forming the conventional smectic A1 phase with a layer thickness corresponding to an average length of the two polymers. In contrast, when two kinds of polymers with the higher *r* values of 1.7−2.8 are mixed, different types of smectic A structures are formed. Upon the addition of the shorter polymer to the abundant longer polymer, a smectic A2 phase in which a pair of smectic layers of shorter polymers nested in a smectic layer of the longer polymers was first formed, and then converted into the smectic A3 phase in which the longer polymers randomly straddled a pair of smectic layers of the shorter polymers. These experimental results are discussed along with a comparison of the theoretical predictions.

Introduction

Liquid crystal phases formed by rod-like molecules have been extensively studied both theoretically and experimentally. Since the initial theoretical studies in the 1950s,[1] it has been shown that systems of hard rod-like particles give rise to the most common liquid crystal sequence of the nematic-smectic-columnar phases based on computer simulations.[2] These phases were formed in the systems of molecules that interact through not only an excluded volume interaction, but also by attractive forces. On the experimental side, we recently reported the predicted phase sequence in the thermotropic liquid crystal (LC) systems of the carefully prepared poly[*n*-decyl-(*S*)-2-methylbutylsilane] (PDMB) with narrow molecular weight distributions,[3] although the columnar and smectic LCs of the rod-like polymers had been separately reported for the lyotropic and thermotropic LCs of synthetic polypeptides,[4] DNA,[5] and some viruses.[6] PDMB is a typical polysilane that forms a thermotropic LC with the following formula:

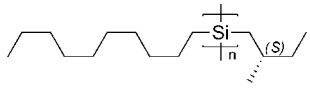

PDMB

This polymer can be considered as an ideal molecule to verify the theoretical predictions of hard rod-like particle systems with an excluded volume interaction because no significant electrostatic interactions are present due to its nonpolar nature. The nonpolar nature is also advantageous for the preparation of a sample with a narrow molecular weight distribution by a simple fractional precipitation method because no aggregation of the polymers takes place in the solution.

Lately, these theoretical and computational approaches have been extended to binary systems of the hard-rod molecules with different length-to-diameter ratios (aspect ratio) to clarify how the two types of rods form the smectic layer.[7] In these theoretical studies, it is of interest to note that the addition of long hard-rod molecules to the abundant half-length molecules stabilizes the smectic A2 phase where the longer molecules are arranged parallel to the director with their center of mass preferentially located in the interstitials between the two layers formed by the shorter molecules. This smectic A2 phase was predicted to be converted into a smectic A phase (called the smectic A1) upon increasing the composition of the longer molecules, which is in equilibrium with the smectic A2 phase over a wide range of mixing ratios. These smectic A2 and A1 phases are rich in shorter molecules and longer molecules, respectively, which is to say that the shorter molecules and longer molecules are typically not miscible, and segregated into two distinct smectic phases.[7e] In contrast, when the lengths of the shorter and longer molecules are similar to each other, both kinds of rods are mixed and settle in the same layer to form the smectic A1 phase.[7a,e]

Although such theoretical predictions of the phase behavior of LC mixtures are of considerable interest to scientists working on condensed matter physics and LC device applications, no conclusive results have been experimentally provided, except that only the smectic phases exhibited by mixtures of conventional molecules composed of aromatic mesogenic groups and aliphatic tail groups have been reported.[8] In this study, we prepared a variety of PDMBs, having a length of 1.96 × *n* Å (*n*: polymerization index) and a diameter of 15 Å, with different molecular weights and narrow molecular weight distributions, and examined how the smectic layer structure is formed in a binary mixture of PDMBs with different lengths.[9]

* To whom correspondence should be addressed. E-mail: kokoshi@polymer.titech.ac.jp.
† Department of Polymer Chemistry, Tokyo Institute of Technology.
‡ Graduate School of Materials Science, Nara Institute of Science and Technology.

10.1021/ma900040x CCC: $40.75
Published on Web 04/21/2009

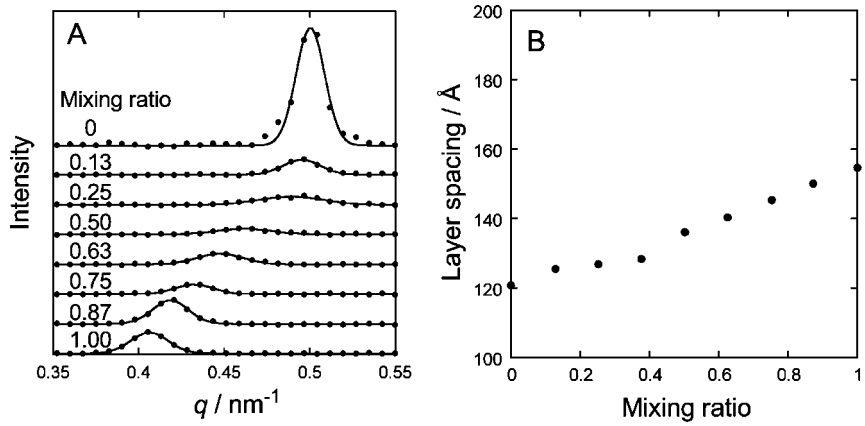

Figure 1. (A) SR-SAXS profiles of the binary mixture of poly-**1** ($M_w = 15.8 \times 10^3$, $M_w/M_n = 1.11$) and poly-$\mathbf{1}_{1.30}$ ($M_w = 20.6 \times 10^3$, $M_w/M_n = 1.10$) of different mixing ratios. (B) Dependence of the observed layer spacings on the mixing ratio of the binary mixture.

Experimental Section

Materials. Chloroform was used as the eluent for the size exclusion chromatography (SEC) measurements, and was of HPLC grade (Wako, Osaka, Japan). Anhydrous chloroform (water content <30 ppm) was purchased from Wako and used for the preparation of the synchrotron radiation small-angle X-ray scattering (SR-SAXS) samples.

Sample Preparation. PDMB was synthesized with the dichlorosilane monomer bearing (*S*)-2-methylbutyl and *n*-decyl substituents by the Wurtz-type condensation in toluene at 120 °C according to previously reported methods.[10] The resulting polymer in toluene was repeatedly fractionated by a fractional precipitation method using 2-propanol, ethanol, and methanol as the precipitants to yield samples with different molecular weights and narrow molecular weight distributions. The PDMBs showed very good solubilities in toluene but were not soluble in the alcohols. The molecular weights of the samples were determined by gel permeation chromatography (GPC) using chloroform at 40 °C as the eluent and with calibration by polystyrene standards. More than 30 samples were prepared that had molecular weights (M_w) ranging from 10000 to 50000 and the molecular weight distributions (M_w/M_n) ranging from 1.05 to 1.15.

Binary Mixtures. Various combinations of the PDMBs were chosen to provide binary mixtures over a wide range of molecular weight ratios and compositions. Here, the PDMB with the lower molecular weight was called poly-**1** as the standard polymer, and a binary mixture was prepared by mixing the higher molecular weight poly-$\mathbf{1}_r$ where the subscript, r (>1), in the sample code represents the molecular weight ratio to the standard poly-**1**. The mixing ratios were given as (weight of poly-$\mathbf{1}_r$/whole weight of the mixture). The polymers were dissolved in chloroform in order to cast the film. The films were annealed in glass capillary tubes at the smectic temperatures of 100−150 °C[3a] for 12 h before the SAXS measurements.

Instruments. The SEC measurements were performed using an LC-2000plus HPLC system (Jasco, Tokyo, Japan) equipped with a GPC K-805 L column (Showa Denko, Tokyo, Japan). Chloroform was used as the eluent at 40 °C at the flow rate of 1 mL/min. The molecular weight calibration curve was obtained using standard polystyrenes (Showa Denko). Polarizing optical microscopic observations were carried out using an Olympus BH-2 polarizing microscope (Olympus, Tokyo, Japan) equipped with a Mettler FP82 hot stage (Mettler-Toledo, Greifensee, Switzerland). The sample was placed on a glass plate covered by a cover glass in order to develop the planar structure in the Mettler hot stage at 100 °C. The SR-SAXS experiments were carried out at the Institute of Materials Structure Science, High Energy Accelerator Research Organization, Tsukuba, Japan (Photon Factory), using small-angle X-ray equipment for solutions installed at beamline BL10C, under the approval of the Photon Factory Advisory Committee (2007G627). Details of the optics and instrumentation are discussed elsewhere.[11]

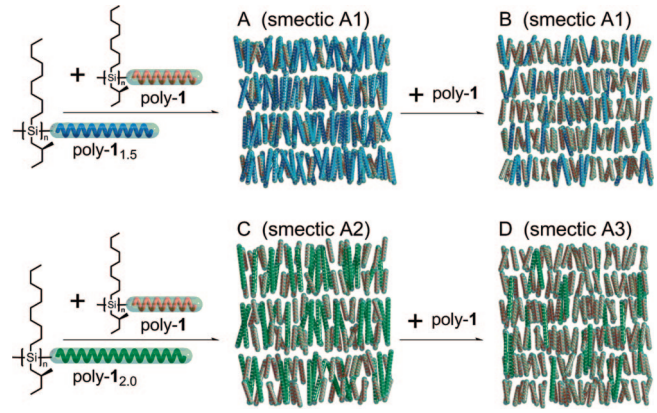

Figure 2. Schematic illustration of smectic phases occurring in binary mixtures of the helical polysilanes with different molecular weights. (A, B) smectic A1 phase as typically formed in the mixture of poly-**1** (A) and poly-$\mathbf{1}_{1.5}$ (B) (blue helices) regardless of the mixing ratio. (C) Smectic A2 phase occurring in the mixture of a small amount of poly-**1** (red helices) and excess poly-$\mathbf{1}_{2.0}$ (green helices). (D) Smectic A3 phase formed upon increasing the addition of poly-**1**.

The incident X-ray intensity of wavelength 0.1488 nm was monitored by an ionization chamber. The samples were kept in glass capillary tubes at 100 °C in a copper heat block with the optical window fixed in the beamline, in which the temperature was regulated within ± 1 °C, during the X-ray exposures. The heat block was set so that the center of the beam coincides with the center of the window of the heat block. The SAXS intensity was collected as the sum of the scattered intensity for 10 min with a one-dimensional position-sensitive proportional counter (PSPC) having 512 channels and the camera length of about 2 m. The number of the counter is connected to the wave vector ($q = (4\pi/\lambda)\sin\theta$) by using the sixth reflection of a collagen, where λ is the wavelength of incident X-ray and 2θ is the scattering angle. The SAXS curves were finally obtained as a function of q followed by normalization for a minor decrease of the primary beam intensity during the measurements, subtraction of the background scattering, and Lorentz correction. The AFM measurements were carried out using a MAC mode III 5500 (Agilent Technology, Inc., Santa Clara, CA) in the AC mode at room temperature under ambient condition. Imaging was conducted in the tapping mode using a silicon cantilever with a resonance frequency of 260 to 320 kHz. The typical settings of the AFM for observations were as follows: set point 3−6 V, scan rate 0.5−1.0 line/s, and scan size 1 × 1 μm^2.

Results and Discussion

Figure 1A shows the typical synchrotron radiation small-angle X-ray scattering (SR-SAXS) profiles observed for the binary

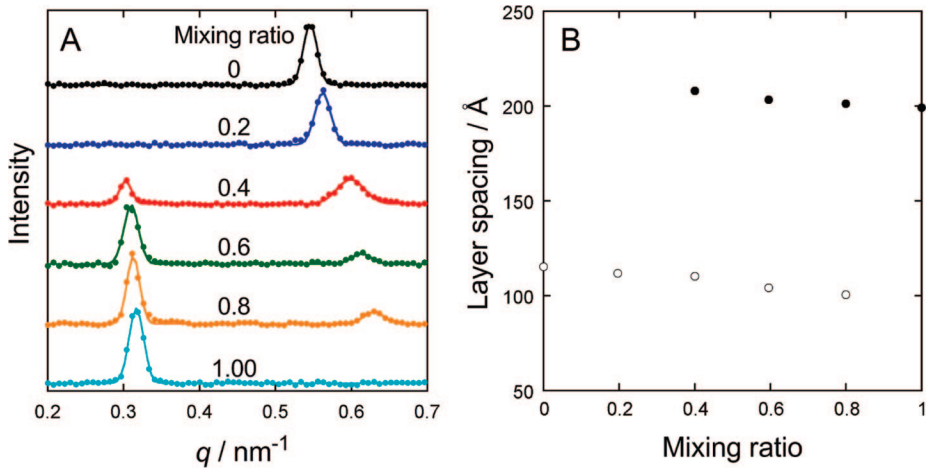

Figure 3. (A) SR-SAXS profiles of the binary mixture of poly-**1** ($M_w = 10.6 \times 10^3$, $M_w/M_n = 1.13$) and poly-$\mathbf{1}_{2.09}$ ($M_w = 22.2 \times 10^3$, $M_w/M_n = 1.15$) as a function of the mixing ratio. The samples were kept at 100 °C in glass capillary tubes during the X-ray exposures. (B) Dependence of the layer spacings observed in the binary mixture of poly-**1** and poly-$\mathbf{1}_{2.09}$ on the mixing ratio.

mixtures of poly-**1** and poly-$\mathbf{1}_{1.30}$ of various mixing ratios. The scattering profiles of poly-**1** and poly-$\mathbf{1}_{1.30}$ showed diffraction peaks with the spacings of 121 and 155 Å, respectively, which correspond to their molecular lengths of 116 and 153 Å calculated using M_n and 1.96 Å as the translational length per residue. Such a good correspondence between the observed spacing and calculated molecular length identifies the smectic A1 structure in which the rod-like molecules are packed into the layer with their long axes perpendicular to the layer.[3a]

Generally, smectic ordering is not favored when the polydispersity of the molecular length is high. This is also the case in our binary mixture system. The layer reflection is significantly weakened or blurred especially for the intermediate mixing ratios as found in Figure 1A, showing a significant decrease in the layer ordering. In Figure 1B, the observed layer spacings are plotted versus the mixing ratio. The observed linear relation indicates that the layer thickness corresponds to the average molecular length. Thus, both the intensity profile and spacing indicate that short and long rod-like molecules are mixed together and accommodated in the same smectic layer as illustrated in Figure 2, parts A and B.

In sharp contrast to these results, the binary mixtures of poly-**1** and poly-$\mathbf{1}_{2.09}$ did not show the conventional dependence of the layer spacing on the mixing ratio, but the reflection peaks at similar positions as observed in the component polymers (see Figure 3A). In Figure 3B, the spacings are plotted versus the mixing ratios. The peak in the small-angle region (or with the large spacing), which may correspond to that of poly-$\mathbf{1}_{2.09}$ ($d =$ 199.1 Å), slightly shifted toward the smaller-angle (larger spacing) direction by adding poly-**1** and disappeared at around the mixing ratio of 0.20. Likewise, the peak in the wide-angle region corresponding to that of poly-**1** ($d = 115.2$ Å) showed a shift toward the wider angle (smaller spacing) direction when increasing the mixing ratio of its counterpart and lasted at around the mixing ratio of 0.80. Thus, two peaks coexist in mixing ratio range from 0.40 to 0.80. These results let us speculate that the two-component polymers are segregated to form each smectic layer, but the fact that the two peaks somewhat shifted from the positions of the individual polymer cannot be explained. A similar behavior is observed in the binary system of poly-**1** and poly-$\mathbf{1}_{2.84}$. Interestingly, this system shows the converse shift in the reflection peaks (see Figures S1A and S1B in the Supporting Information).

To clarify the reason for the peak shift, we carried out a series of SR-SAXS measurements of the various binary mixtures of poly-**1** and poly-$\mathbf{1}_r$ with r ranging from 1.88 to 2.76 at the

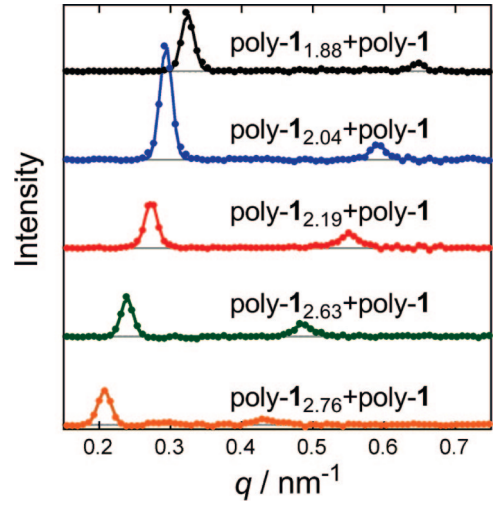

Figure 4. SR-SAXS profiles of the binary mixture of poly-**1** ($M_w = 13.5 \times 10^3$, $M_w/M_n = 1.06$) and poly-$\mathbf{1}_r$s (poly-$\mathbf{1}_{1.88}$ ($M_w = 25.4 \times 10^3$, $M_w/M_n = 1.09$), poly-$\mathbf{1}_{2.04}$ ($M_w = 27.6 \times 10^3$, $M_w/M_n = 1.08$), poly-$\mathbf{1}_{2.19}$ ($M_w = 29.6 \times 10^3$, $M_w/M_n = 1.10$), poly-$\mathbf{1}_{2.63}$ ($M_w = 35.5 \times 10^3$, $M_w/M_n = 1.09$), and poly-$\mathbf{1}_{2.76}$ ($M_w = 37.3 \times 10^3$, $M_w/M_n = 1.11$)) at a mixing ratio of 0.75.

constant mixing ratio of 0.75. Here, the same sample was used as the standard poly-**1**, and poly-$\mathbf{1}_r$ was varied. The results are shown in Figure 4. A two-peak profile is observed for all the mixtures. Of interest is the peak shift by changing r. The reflection in the smaller angle region locates at a position similar to that for poly-$\mathbf{1}_r$. However, the other one in the wide angle region does not correspond to that of poly-**1**; irrespective of the use of the same poly-**1**, its spacing increased with an increase in the molecular weight of the counterpart poly-$\mathbf{1}_r$. The latter fact means that the appearance of two peaks is not due to the simple demixing of poly-**1** and poly-$\mathbf{1}_r$ into two smectic phases. By careful observation of Figure 4, we noticed that the reflection in the wide angle region is of the second order of the small angle reflection, in other words, it is indexed to the (002) reflection.

We now question why the smectic phase in the mixture can show the second (002) reflection despite the fact that the smectic phase in each component polymer shows only a first (001) reflection (refer to Figures 3A and S1A). The only plausible explanation for this is the formation of a smectic A2 layer structure, as schematically depicted in Figure 2C where a pair of smectic layers of shorter molecules (poly-**1**) is nested in a

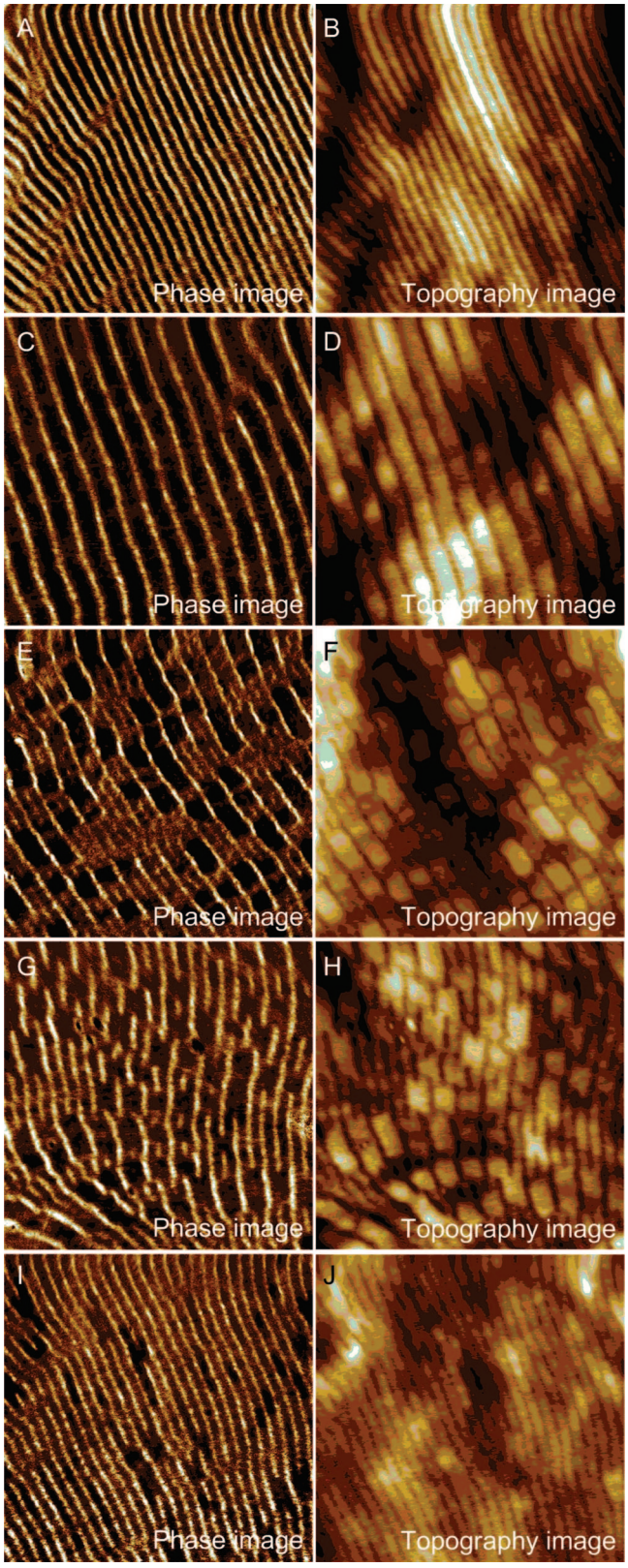

Figure 5. AFM images observed on the film surface of poly-**1**s. (A, B) poly-**1** ($M_w = 53.8 \times 10^3$, $M_w/M_n = 1.17$), (C, D) poly-$\mathbf{1}_{2.49}$ ($M_w = 134.0 \times 10^3$, $M_w/M_n = 1.30$), and (E-J) the binary mixture of poly-**1** and poly-$\mathbf{1}_{2.49}$ at a mixing ratio of 0.75 (E, F), 0.50 (G, H), and 0.33 (I, J). The film samples with thicknesses of 20−50 μm were cast on glass plates from the corresponding chloroform solutions, annealed for 1 h at 140 °C and then quenched to room temperature. Scale = 1000 × 1000 nm.

smectic layer of longer molecules (poly-$\mathbf{1}_r$). Such a molecular arrangement forms a low electron density part in the central part of the longer molecular layer so that the strong intensity

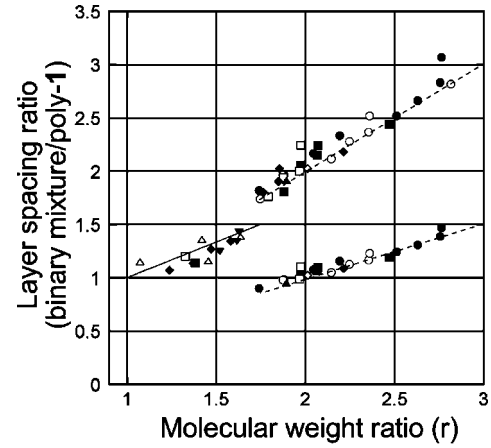

Figure 6. Dependence of the observed layer spacing ratio (binary mixture/poly-**1**) on the molecular weight ratio, r, of the binary mixture of poly-$\mathbf{1}_r$ and poly-**1** at the mixing ratio of 0.75. The solid and dashed lines are calculated on the basis of the smectic A1 structure and smectic A2 structure, respectively (refer to the text). The circles, squares, triangles, and diamonds represent each polymer selected as the standard poly-**1**.

can be expected for the second (002) reflection to be similar to the first (001) reflection. Furthermore, the increase in the smectic layer spacing with the mixing ratio of the shorter poly-**1** in Figure 3B is reasonable, because the layer spacing should be the average of the smectic layer spacing of the longer poly-$\mathbf{1}_{2.09}$ (199.1 Å) and double that of the shorter poly-**1** (115.2 × 2 Å). By the same reason, the opposite trend observed in Figure S1 is reasonable since, in this case, the layer spacing of the longer poly-$\mathbf{1}_{2.84}$ (350.5 Å) is greater than double that of the shorter poly-**1** (143.4 × 2 Å).

The characteristic layer structure in the smectic A2 phase was also supported by the AFM observations, which have been found to be an excellent way to collect information on the smectic layer order and spacing.[12] Figure 5 shows the AFM images of the films of poly-**1** (A, B), poly-$\mathbf{1}_{2.49}$ (C, D) and their binary mixtures at the mixing ratios of 0.75 (E, F), 0.50 (G, H), and 0.33 (I, J). One can see a very clear banding topography characteristic of the repeating smectic layer. The observed bandings in Figure 5A, B and Figure 5C, D show the repeat distances of 38.3 and 78.2 nm, respectively, which are approximately equal to the molecular lengths of the corresponding polymers. In the binary mixture of poly-**1** and poly-$\mathbf{1}_{2.49}$ at the mixing ratio of 0.75 in Figure 5E, F, the wide bandings (81.8 nm) were observed to be split in two by narrow bandings (40.9 nm), clearly reproducing the schematic illustration of the smectic A2 phase in Figure 2C.

It should be noted that the wide bands due to poly-$\mathbf{1}_{2.49}$ are also observed at the mixing ratio of 0.50 in Figure 5G, H. However, they are occasionally jolted out of alignment by a half-banding pitch. As a result, the wide banding has only the short correlation length in directions both parallel and perpendicular to the layer, leading to the disappearance of the (001) reflection as observed in Figures 3A and S1A. At the mixing ratio of 0.33, almost all of the wide bandings are converted into the narrow banding of poly-**1** in Figure 5I, J. This may be due to the essential change in the molecular arrangement within a layer. Probably, the longer poly-$\mathbf{1}_r$ may randomly straddle a pair of smectic layers of poly-**1** as schematically depicted in Figure 2D. This is also a novel type of smectic phase, the so-called smectic A3.

Finally, we refer to the question of why the binary mixtures prefer the smectic A2 structure to the random mixing smectic A1 structure. To answer this, we examined the X-ray analysis of the various binary mixtures with molecular weight ratios of

$1 < r < 3$. Here, the polymers with the various molecular weights of 10,000 to 18,000 were selected as the standard poly-**1** and the mixing ratio of 0.75 (i.e., with longer poly-$\mathbf{1}_r$ in abundance) was selected because of the limited amount of each sample. In Figure 6, the ratios of the observed spacing of the binary mixture to that of the standard poly-**1** are plotted versus the molecular weight ratios. For $1.0 < r < 1.7$ (that is, the difference in length between two polymers is relatively smaller), only one reflection is observed. The layer spacing ratio corresponds to the calculated one (solid line) from the molecular weight ratio and mixing ratio under the assumption that short and long molecules are mixed together. In this range of r, hence, the smectic A1 phase is formed with the layer spacing of the average molecular length as has been theoretically predicted.[7e] In contrast, the binary mixtures for $1.7 < r < 2.8$ show two reflections, the first and second reflections, and then form the smectic A2. Their spacing ratios also correspond to the calculated ones (dashed lines) based on the smectic A2 structure. The smectic A2 for $1.7 < r < 2.8$ is also theoretically predicted, but its appearance in the composition with shorter molecules in large abundance[7e] does not coincide with the observation in which the smectic A2 appears in the composition with the longer molecules in high abundance.

Conclusions

In conclusion, three types of smectic phases with different accommodations for two polymers are formed. In the binary mixture of the shorter and longer polymers with the longer molecular weight ratio (r) from 1.0 to 1.7 ($1.0 < r < 1.7$), the two polymers are randomly mixed within a layer forming the conventional smectic A1 phase with a layer thickness corresponding to the average length of the two polymers. In contrast, when two kinds of polymers with the higher molecular weight ratio (r) of 1.7 to 2.8 ($1.7 < r < 2.8$) are mixed, different types of smectic A structures are formed. Upon the addition of the shorter polymer to the abundant longer polymer, a smectic A2 layer in which a pair of smectic layers of shorter polymers nested in a smectic layer of the longer polymers was first formed, and then converted into a smectic A3 phase in which the longer polymer randomly straddled a pair of smectic layers of shorter polymers. The binary mixtures of the poly-**1**s are ideal systems for comparison with the theoretical results of several binary mixtures of hard spherocylinders of the same diameter and different lengths, which will not only provide a good test for the theoretical treatments, but also open the way for the realization of the predictions for rod-like particle mixtures with a well-defined bidispersity, notwithstanding the crudeness of the theory. In particular, it will be worth implementing the experimental studies on the nature of the phase transition of such smectic phases of the bidisperse rod-like polymers upon temperature and pressure changes for the purpose of understanding the self-organization of molecules. Some of the projects outlined above will be the object of future investigations. The present results demonstrate how to manipulate the processing of nanoscaled materials for use in the areas of optical devices and sensors, which might be relevant to systems of amphiphiles, block copolymers, and composite materials.

Acknowledgment. This research was supported by a Grant-in-Aid for Creative Research from the Ministry of Education, Science, and Culture in Japan.

Supporting Information Available: Figures showing additional experimental results (SR-SAXS profiles and observed layer spacings of the binary mixture of poly-**1** and poly-$\mathbf{1}_{2.84}$ as a function of the mixing ratio, and polarized optical micrograph of the binary mixture of poly-**1** and poly-$\mathbf{1}_{2.04}$ in a parallel glass cell). This material is available free of charge via the Internet at http://pubs.acs.org.

References and Notes

(1) (a) Onsager, L. *Ann. N.Y. Acad. Sci.* **1949**, *51*, 627–659. (b) Saupe, A.; Maier, W. *Z. Naturforsch.* **1958**, *13a*, 564–566.
(2) (a) Stroobants, A.; Lekkerkerker, H. N. W.; Frenkel, D. *Phys. Rev. Lett.* **1986**, *57*, 1452–1455. (b) Stroobants, A.; Lekkerkerker, H. N. W.; Frenkel, D. *Phys. Rev. A* **1987**, *36*, 2929–2945. (c) McMillan, W. L. *Phys. Rev. A* **1971**, *4*, 1238–1246. (d) Kobayashi, K. K. *Mol, Cryst. Liq. Cryst.* **1971**, *13*, 137–48.
(3) (a) Okoshi, K.; Kamee, H.; Suzaki, G.; Tokita, M.; Fujiki, M.; Watanabe, J. *Macromolecules* **2002**, *35*, 4556–4559. (b) Okoshi, K.; Saxena, A.; Fujiki, M.; Suzaki, G.; Watanabe, J.; Tokita, M. *Mol. Cryst. Liq. Cryst.* **2004**, *419*, 57–68. (c) Okoshi, K.; Saxena, A.; Naito, M.; Suzaki, G.; Tokita, M.; Watanabe, J.; Fujiki, M. *Liq. Cryst.* **2004**, *31*, 279–283.
(4) (a) Livolant, F.; Bouligand, Y. *J. Phys. (Paris)* **1986**, *47*, 1813–1827. (b) Lee, S.-D.; Meyer, R. B. *Liq. Cryst.* **1990**, *7*, 451–455. (c) Watanabe, J. In *Ordering in Macromolecular Systems*; Teramoto, A., Kobayashi, M., Norisue, T., Eds.; Springer: Berlin, 1993; p 99. (d) Watanabe, J.; Takashina, Y. *Macromolecules* **1991**, *24*, 3423–3426. (e) Yu, S. M.; Conticello, V. P.; Zhang, G.; Kayser, C.; Fournier, M. J.; Mason, T. L.; Tirrell, D. A. *Nature (London)* **1997**, *389*, 167–170. (f) Okoshi, K.; Sano, N.; Suzuki, G.; Kamee, H.; Tokita, M.; Magoshi, J.; Watanabe, J. *Jpn. J. Appl. Phys.* **2002**, *41*, L720–L722. (g) Yen, C.-C.; Edo, S.; Oka, H.; Tokita, M.; Watanabe, J. *Macromolecules* **2008**, *41*, 3727–3733.
(5) (a) Strzelecka, T. E.; Davidson, M. W.; Rill, R. L. *Nature (London)* **1988**, *331*, 457–460. (b) Livolant, F.; Levelut, A. M.; Doucet, J.; Benoit, J. P. *Nature (London)* **1989**, *339*, 724–726.
(6) (a) Wen, X.; Meyer, R. B.; Casper, D. L. D. *Phys. Rev. Lett.* **1989**, *63*, 2760–2763. (b) Dogic, Z.; Fraden, S. *Phys. Rev. Lett.* **1997**, *78*, 2417–2420. (c) Lee, S.-W.; Mao, C.; Flynn, C. E.; Belcher, A. M. *Science* **2002**, *296*, 892–895. (d) Lee, S.-W.; Wood, B. M.; Belcher, A. M. *Langmuir* **2003**, *19*, 1592–1598. (e) Tomar, S.; Green, M. M.; Day, L. A. *J. Am. Chem. Soc.* **2007**, *129*, 3367–3375.
(7) (a) Koda, T.; Kimura, H. *J. Phys. Soc. Jpn.* **1994**, *63*, 984–994. (b) Cui, S. M.; Chen, Z. Y. *Phys. Rev. E* **1994**, *50*, 3747–3754. (c) Sear, R. P.; Jackson, G. *J. Chem. Phys.* **1995**, *102*, 2622–2627. (d) Van Roij, R.; Mulder, B. *Phys. Rev. E* **1996**, *54*, 6430–6440. (e) Cinacchi, G.; Mederos, L.; Velasco, E. *J. Chem. Phys.* **2004**, *121*, 3854–3863.
(8) Sigaud, G.; Hardouin, F.; Achard, M. F.; Gasparoux, H. *J. Phys. Colloq.* **1979**, *40* (C3), 356–359.
(9) Even though we fully understood that such an optically active helical polymer leads to a further macroscopic chirality in the liquid crystal state, it seemed to be appropriate to conduct the research with PDMB because this polymer is very stiff and its liquid crystalline phase behavior is well understood.[3]
(10) Fujiki, M. *J. Am. Chem. Soc.* **1996**, *118*, 7424–7425.
(11) Ueki, T.; Hiragi, Y.; Kataoka, M.; Inoko, Y.; Amemiya, Y.; Izumi, Y.; Tagawa, H.; Muroga, Y. *Biophys. Chem.* **1985**, *23*, 115–124.
(12) Oka, H.; Suzaki, G.; Edo, S.; Suzuki, A.; Tokita, M.; Watanabe, J. *Macromolecules*, **2008**, *41*, 7783−7786. The molecular weights of the samples used for the AFM observations were much higher than those used in the SR-SAXS measurements because the bandings observed in the samples with the molecular weight of 10−30k were too narrow and barely recognizable by our AFM apparatus.

MA900040X